Res Chem Intermed (2017) 43:911–926
DOI 10.1007/s11164-016-2673-x

Synthesis of CuO from $CuCO_3 \cdot Cu(OH)_2$ and its catalytic activity in the degradation of methylene blue

Bowen Xue[1] · Chang Qv[1] · Zhongwen Qian[1] · Chunyu Han[1] · Genxiang Luo[1]

Received: 2 April 2016 / Accepted: 22 July 2016 / Published online: 28 July 2016

Abstract A one-step route has been designed to synthesize CuO nanostructures using basic cupric carbonate ($CuCO_3 \cdot Cu(OH)_2$) as a precursor. The crystal structure and phase purity of as-obtained CuO was characterized by X-ray diffraction. The elemental compositions of samples were analyzed by energy-dispersive X-ray spectroscopy. Scanning electron microscopy and transmission electron microscopy were used to analyze the structure and morphology of as-obtained CuO. The bandgap energy of CuO particles produced was assessed by UV–Vis spectroscopy. The possible formation processes of CuO are discussed. Furthermore, the catalytic activity of prepared CuO particles was investigated in the degradation of methylene blue.

Keywords $CuCO_3 \cdot Cu(OH)_2$ · CuO · Synthesis · Catalytic activity · Degradation · Methylene blue

Introduction

Wastewater combined with a variety of organic compounds especially dyestuffs is the source of environmental contamination [1]. The primary part of organic compounds is aromatic compounds, particularly sulfo, nitro, amidocyanogen, or chloro series [2]. Methylene blue (MB) is a heterocyclic aromatic chemical compound used in industry for dying, e.g. cotton, wool, acrylic, silk [3, 4]. Photocatalytic degradation is a much more efficient way to treat wastewater. Therefore, photocatalysts play an important role in the degradation of organic

---

✉ Genxiang Luo
gxluo1965@163.com

[1] School of Chemistry and Materials Science, Liaoning Shihua University, Fushun 113001, People's Republic of China

compounds. Various types of photocatalysts, including WO_3 [5], TiO_2 [6–8], ZnO [9], ZnS [10], CuS [11], and composited semiconductors [12–27], were prepared to catalyze the degradation of organic contaminations.

Copper oxide (CuO) is a significant p-type semiconductor with a narrow bandgap, which has been widely applied in many potential fields, such as supercapacitors, sensors, solar cells, photodetectors, catalysis, enhancement of thermal conductivity of nano-fluids, field emission displays (FED), superhydrophobic surfaces, photocatalysis [28–31]. CuO has some features that make it suitable to be a photocatalyst, such as low cost, photocatalytic activity, reusability, nontoxicity, and abundant resources etc. [32, 33].

Because of the wide applications of CuO, many researchers have focused on discovering new methods of synthesising CuO. Several chemical synthesis methods of CuO were reported, including wet chemistry [34], electrochemical [35], microwave irradiation [36], ultrasonic waves [37], precipitation [38], and hydrothermal [39–42]. Most of these methods effectively control the synthesis of prepared CuO powders. However, some methods sometimes need multistep reactions and high temperature. Therefore, it is a challenge to design a low temperature and simple route for the synthesis of CuO.

Different copper sources, including $Cu(OH)_2$ [43], $Cu(CH_3COO)_2{\cdot}2H_2O$ [44], $Cu(NO_3)_2{\cdot}3H_2O$ [34], $CuCl_2{\cdot}2H_2O$ [45], $Cu_2(OH)_3NO_3$ [46], $Cu_2(OH)_3Cl$ [47, 48], $Cu_4SO_4(OH)_6$ [49, 50] $CuCO_3{\cdot}Cu(OH)_2$ [51–53], have been used as precursors or intermediates for the preparation of CuO. Among the copper sources, $CuCO_3$-$Cu(OH)_2$ widely exists in natural ores, so it is plentiful, cheap, and easier to be achieved. Zhang et al. [51] and Zhu et al. [52] used $CuCO_3{\cdot}Cu(OH)_2$ as a precursor to fabricate CuO via calcination. Wang et al. [53] used $CuCO_3{\cdot}Cu(OH)_2$ as precursor and H_2O_2 aqueous solution as an additive for the preparation of CuO via hydrothermal method.

In this paper, a mild alkaline condition was adopted to produce CuO, which was obtained by the dehydration of $Cu(OH)_2$ intermediate from the precursor of $CuCO_3{\cdot}Cu(OH)_2$. A series of control experiments were carried out to investigate the influencing factors and the possible formation processes of as-obtained CuO particles. The catalytic activity of CuO was tested by the degradation of MB.

Experimental

Materials

Chemicals including $CuCO_3{\cdot}Cu(OH)_2$, NaOH, MB, H_2O_2 aqueous solution, anhydrous ethanol were all of analytical grade and used in this work without any further purification. Distilled water was used throughout the experiments.

Synthesis of CuO

A quantity of 2.21 g $CuCO_3{\cdot}Cu(OH)_2$ powder was added into NaOH aqueous solution (40 mL 0.5 M) at a stoichiometric ratio of 1:2 in a beaker under constant stirring. The beaker was sealed and heated at 80 °C for 6 h. After the reaction was finished, the black precipitate was collected by centrifugation and washed with distilled water and anhydrous ethanol several times. Finally, the precipitate was dried in an infrared drying oven. By using single factor experiment, synthesis condition was optimized. The details of reactants and reaction conditions are shown in Table 1. The schematic of synthesis processes was shown in Fig. 1.

Characterization

The crystallographic structure of the products prepared was characterized by X-ray diffraction (XRD, D/max-RB 12 kW) with CuKα radiation ($\lambda = 0.15418$ nm), operating at 40 kV and 100 mA, and the diffraction patterns were carried out in the range of $10° < 2\theta < 70°$. The Debye–Scherrer equation is used to calculate the particle size of CuO powder:

$$D = \frac{k\lambda}{\beta \cos\theta} \tag{1}$$

where D is the mean size of the particles, k is a dimensionless shape factor (0.89) with a value close to unity, and λ is the X-ray wavelength (0.15418 nm), and β is the line broadening at half the maximum (FWHM) of the diffraction peak, and θ is the Bragg angle.

The varieties and contents of elements in samples were analyzed by JSM-7500F energy-dispersive X-ray spectroscopy (EDX, JEOL, Japan). The surface morphology of the as-prepared samples was analyzed by a SU800 scanning electron microscope (SEM, Hitachi, Japan). Transmission electron microscopy (TEM) images were performed on a JEOL 2200FS (200 kV) transmission electron microscope.

Table 1 The details of reactants and reaction conditions

Entry	$CuCO_3 \cdot Cu(OH)_2$ (mol)	NaOH (mol L^{-1})	pH	Reaction temperature (°C)	Reaction time (h)
A	0.01	0.5	13.7	80	6
B	0.01	0.5	13.7	70	6
C	0.01	0.5	13.7	60	6
D	0.01	0.5	13.7	50	6
E	0.01	0.5	13.7	40	6
F	0.01	0.5	13.7	25	6
G	0.01	0.5	13.7	50	5
H	0.01	0.5	13.7	50	4
I	0.01	0.5	13.7	50	3
J	0.005	0.1	13.0	50	5
K	0.005	0.05	12.7	50	5
L	0.005	0.025	12.4	50	5

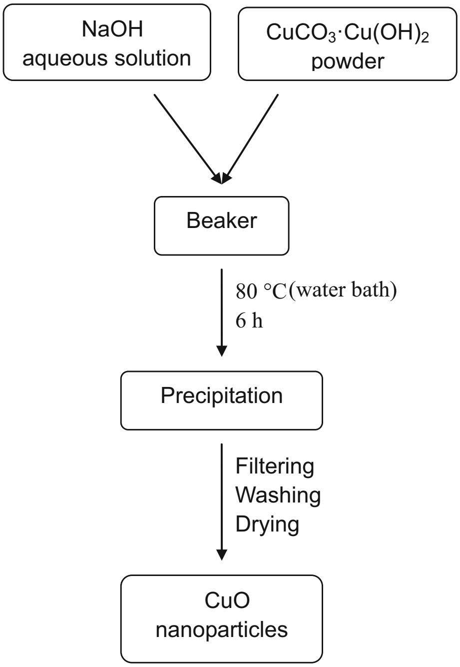

Fig. 1 Schematic of the experimental procedure

UV–Vis diffuse reflectance spectra (DRS) were performed by Agilent Cary 5000 UV–Vis spectrophotometer at room temperature.

Photocatalytic experiment

In the photocatalytic experiment, MB was used to assess the photocatalytic performance of the as-prepared CuO samples. An aqueous solution of 0.140 mol L^{-1} H_2O_2 and 0.01 g of CuO samples were added to 70 mL of original dye (10 mg L^{-1}). The solution was stirred at room temperature. In the first 10 min, the solution was kept in dark conditions to achieve adsorption equilibrium. After that, the solution was continuously stirred and irradiated with a 125 W Hg lamp at irradiation wavelength 365 nm at room temperature. The lamp was 20 cm above the surface of the solution. During the whole experimental process, the solution was sampled and centrifuged to separate the catalyst at given time. The supernatants were analyzed by UV–Vis spectrophotometer (UNICO UV-2000) to obtain the absorbance value of different reaction time at 664 nm. Meanwhile, the degradation efficiency formula is given by Eq. (2),

$$\eta = \frac{(A_0 - A)}{A_0} \times 100\,\%, \tag{2}$$

where η is the degradation efficiency (%), A_0 is the initial absorbance of dye, A is the absorbance of dye after the irradiation.

Results and discussion

Nanoparticle characterization

The crystallographic structures of the as-prepared CuO particles with different temperatures, reaction time, and alkali concentrations were characterized by XRD in Figs. 2, 3, and 4, respectively. In Fig. 2, $CuCO_3 \cdot Cu(OH)_2$ and NaOH solution (0.5 M) were heated at different temperatures (25, 40, 50, 60, 70, and 80 °C) for 6 h. When the temperature is below 40 °C, the diffraction peaks contain impure peaks. $Cu(OH)_2$ was not converted into CuO completely. When the temperature goes up, all of the diffraction peaks in the XRD patterns of the as-obtained samples agree with the standard CuO XRD pattern, for which the 2θ values of 32.488, 35.550, 38.667, 48.840, 53.398, 58.204, 61.578 could be indexed to the (h k l) indices (1 1 0), (−1 1 1), (1 1 1), (−2 0 2), (0 2 0), (2 0 2), and (−1 1 3), respectively. Therefore, the minimum transition temperature of $CuCO_3 \cdot Cu(OH)_2$ to CuO is 50 °C, which is in good agreement with that reported in the literature [54].

In Fig. 3, $CuCO_3 \cdot Cu(OH)_2$ and NaOH solution (0.5 M) were heated at 50 °C for different reaction times (3, 4, 5, and 6 h). The diffraction peaks of samples that were synthesized at 5 and 6 h can be indexed to the standard monoclinic structures of CuO crystal in great agreement with JCPDS No. (89-2529) without any characteristic peaks of impurities, such as $Cu(OH)_2$ and $CuCO_3 \cdot Cu(OH)_2$. When the reaction time is <5 h, impure peaks exist in the diffraction pattern.

In Fig. 4, $CuCO_3 \cdot Cu(OH)_2$ and NaOH solution with different concentration (0.025, 0.05, 0.1, and 0.5 M) were heated at 50 °C for 5 h. The stronger diffraction peaks of the three samples agree well with the standard CuO XRD pattern. Among the investigated alkali concentration, CuO could be synthesized as long as the molar ratio of $CuCO_3 \cdot Cu(OH)_2$ and NaOH is 1:2.

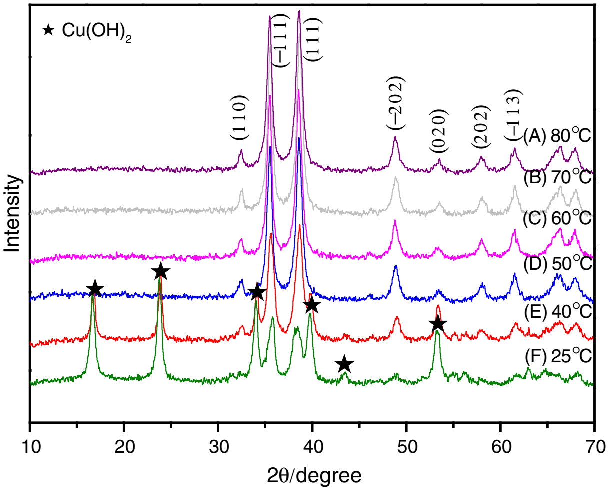

Fig. 2 XRD patterns of CuO produced with different temperatures

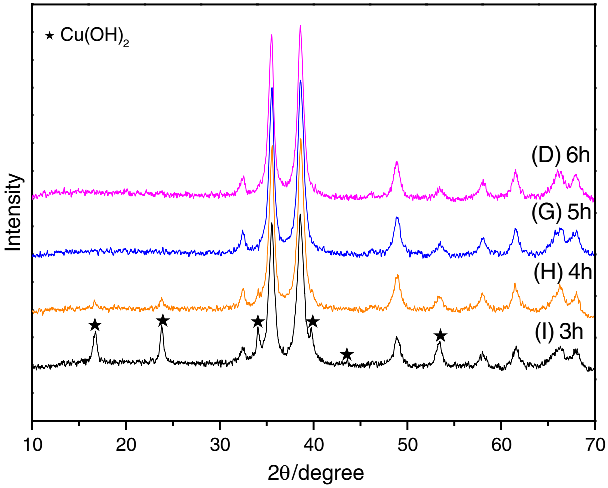

Fig. 3 XRD patterns of CuO produced with different reaction time

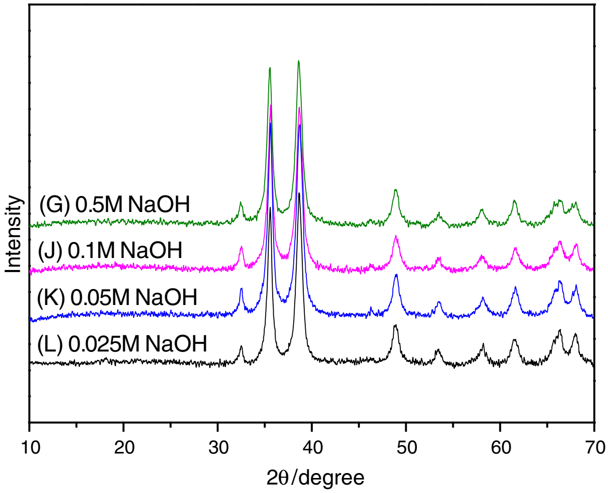

Fig. 4 XRD patterns of CuO produced with different concentrations of NaOH

Considering the volume of solution, 0.1 M NaOH solution is more appropriate. The optimal condition of CuO synthesis is as follows: the molar ratio of $CuCO_3 \cdot Cu(OH)_2$ and NaOH is 1:2 with 0.1 M of NaOH at 50 °C for 5 h. The grain size of CuO in the optimal condition is 13.6 nm which is calculated by Debye–Scherrer equation. According to the investigation of reaction conditions, the formation process of CuO could be inferred as follows:

$$CuCO_3 \cdot Cu(OH)_2 + 2NaOH \rightarrow 2Cu(OH)_2 + Na_2CO_3 \tag{3}$$

$$2Cu(OH)_2 \rightarrow 2CuO + 2H_2O \tag{4}$$

After $CuCO_3{\cdot}Cu(OH)_2$ and NaOH aqueous solution mixed, $Cu(OH)_2$ and Na_2CO_3 was produced at the beginning. Then $Cu(OH)_2$ was dehydrated into CuO and H_2O. The overall reaction was shown as follows:

$$CuCO_3 \cdot Cu(OH)_2 + 2NaOH \rightarrow 2CuO + Na_2CO_3 + 2H_2O \tag{5}$$

Besides CuO, Na_2CO_3, an important raw material in chemical manufacture, can be obtained by recrystallization.

The EDX spectra of the elemental compositions of CuO nanoparticles is shown in Fig. 5. The atomic ratio of Cu to O is 1.04:1, which is close to the theoretical stoichiometry of CuO (Cu:O = 1:1). The existence of C originates from conductive tape.

Figure 6 shows the scanning electron microscopy (SEM) of as-prepared CuO. Figure 6a, the low-magnification SEM image, indicates that the as-prepared CuO nanostructures are sphere-like. To further examine the microstructure of the microspheres, the high-magnification SEM (Fig. 6b) image was recorded. The sphere-like nanostructures were actually constituted by numerous small nanoplates. The diameter range of microsphere is about 11.75–12.68 μm.

The morphology and crystallographic characterization of the as-prepared CuO microsphere were further characterized by TEM (Fig. 7). It can be seen that the sphere-like products are composed of nanosheets, and some of these nanosheets have joined together and disorderly attached to form hierarchical features. It can be seen that the nanoplates which compose CuO microsphere is about 10 nm in thickness.

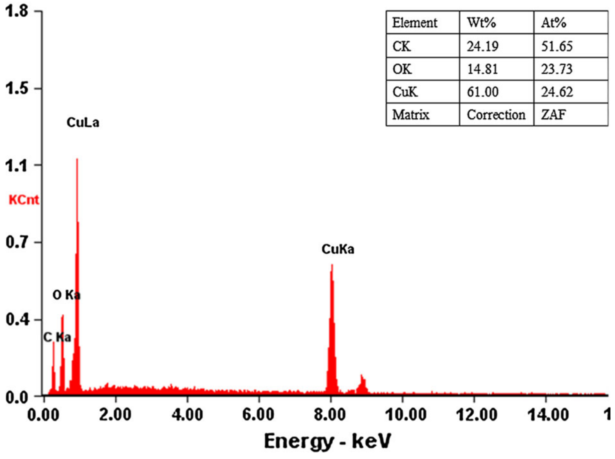

Element	Wt%	At%
CK	24.19	51.65
OK	14.81	23.73
CuK	61.00	24.62
Matrix	Correction	ZAF

Fig. 5 EDX spectra of the CuO samples

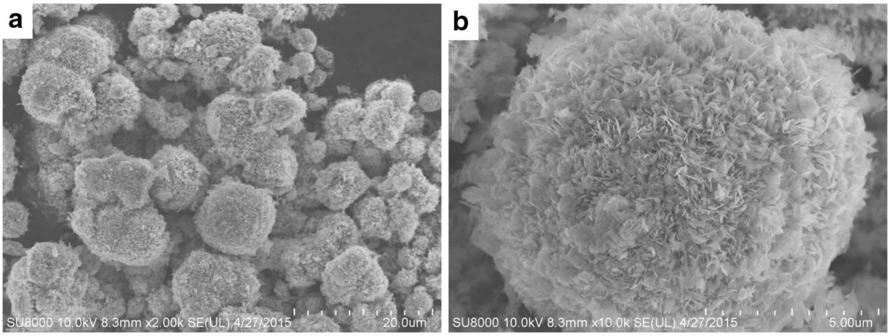

Fig. 6 SEM images of CuO sample prepared at optimal synthesis condition

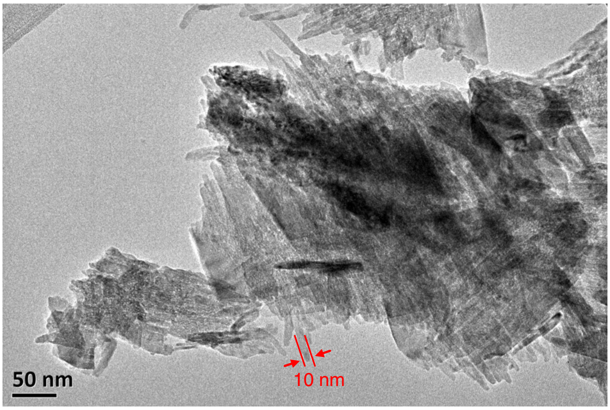

Fig. 7 TEM image of CuO sample prepared at optimal synthesis condition

The UV–Vis DRS of the as-prepared CuO samples was shown in Fig. 8. It has a broad absorption peak at about 394 nm. In addition, the optically wide direct band gap of the CuO particles from the spectrum can be evaluated by the following equation:

$$(\alpha h\upsilon)^n = \mathrm{A}\left(h\upsilon - E_g\right) \tag{6}$$

where $h\upsilon$ is the photon energy, α is the absorption coefficient, A is a constant relative to the material and the matrix element of the transition and n is either 2 for a direct electronic transition or 1/2 for an indirect electronic transition. CuO is direct electronic transition, so n is equal to 2. The inserted spectrum was the best linear relationship of plotting $(\alpha h\upsilon)^2$ and $h\upsilon$. The straight line to the x axis ($\alpha = 0$) is the optical absorption edge energy of the as-obtained CuO. The band gap (E_g) value is about 1.92 eV which is larger than the normal value of bulk CuO ($E_g = 1.85$ eV). The result shows a blue shift in band gap energy with respect to the corresponding bulk CuO. The increase of the band gap is ascribed to the quantum size confinement effects for semiconductors [55, 56]. Similar results have been obtained from CuO

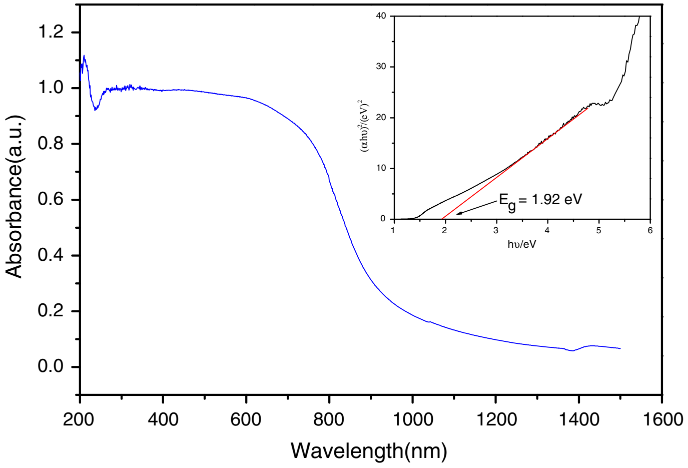

Fig. 8 UV–Vis DRS of CuO sample prepared at optimal synthesis condition

nanoflakes (2.15 eV) [53], CuO nanoparticles (2.43 eV) [55], and CuO nanowires (3.48 eV) [57].

Photocatalytic activity

The catalytic activity of the as-obtained CuO samples was estimated by the degradation of MB at room temperature. In Fig. 9, the degradation efficiency of MB is only 1.78 % in the absence of H_2O_2. While in the presence of H_2O_2, the degradation efficiency is much higher (98.78 %). Therefore, H_2O_2 is a necessary factor for the photocatalysis experiment.

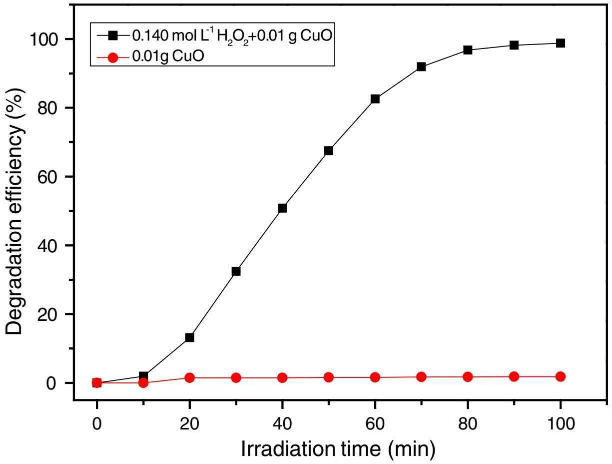

Fig. 9 Effect of the presence of H_2O_2; [MB] = 10 mg L^{-1}

The degradation efficiencies of MB versus concentration of H_2O_2 (Fig. 10) with 0.01 g CuO are almost the same in 100 min, but there is much difference in the degradation rate. The degradation of MB dye follows a first-order kinetic process, which declines linearly in the reaction. The kinetic equation is given by Eq. (7) [58, 59],

$$\ln\left(\frac{C}{C_0}\right) = -kt, \tag{7}$$

where C_0 is the initial concentration of reactants, C is the concentration of reactants, k is the first-order reaction rate constant, t is the reaction time. Because the concentration of reactants is proportional to the absorbance, C/C_0 is equivalent to A/A_0. The variation trend of kinetic slope is equal to the variation trend of reaction rate constant. Increasing the concentration of H_2O_2, more $^{\cdot}OH$ radicals were produced. However, when the concentration of H_2O_2 exceeds optimal concentration, the degradation rate will decrease. Because H_2O_2 react with $^{\cdot}OH$ radicals to scavenge $^{\cdot}OH$ radicals at higher concentration of H_2O_2, which is shown in Eqs. (8) and (9) [58, 60].

$$HO^{\cdot} + H_2O_2 \rightarrow H_2O + HO_2^{\cdot} \tag{8}$$

$$HO_2^{\cdot} + HO^{\cdot} \rightarrow H_2O + O_2. \tag{9}$$

Figure 11 illustrates the degradation efficiency and the degradation kinetics of MB versus different CuO dosage. Compared with the absence of CuO, the degradation efficiency increased obviously with the presence of CuO. So CuO is an effective catalyst in the photodegradation of MB. With the increase of CuO dosage, the slope of straight line goes up gradually. Because of the increased CuO dosage, both the adsorption of UV-light and the formation of active species were improved. When the dosage of CuO is excessive, the degradation efficiency is decreased because of the aggregation of solid particles [61–64].

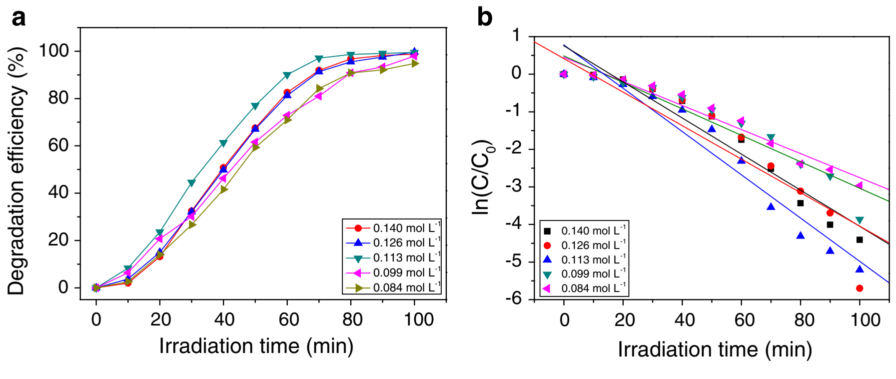

Fig. 10 Degradation of MB versus concentration of H_2O_2 (**a**) and photodegradation kinetics of MB (**b**); [MB] = 10 mg L^{-1}; $m_{CuO} = 0.01$ g

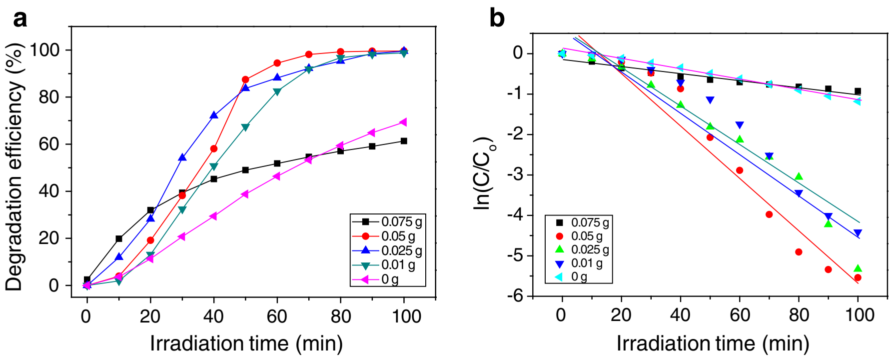

Fig. 11 Degradation of MB versus CuO dosage (**a**) and photodegradation kinetics of MB (**b**); $[MB] = 10$ mg L^{-1}; $H_2O_2 = 0.140$ mol L^{-1}

The effect of initial dye concentration on the degradation of MB was investigated under irradiation. The range of MB concentration was changed from 5 to 15 ppm. The degradation efficiency and photodegradation kinetics were shown in Fig. 12. When the MB concentration is increased, the degradation efficiency was reduced. With the increase of dye concentration, much more dye molecules were adsorbed on the surface of CuO. The dye molecules which adsorbed on the catalyst surface hinder the adsorption of OH^- ions and decrease the active sites for the adsorption of OH^- ions. It leads to the reduction of the formation of $^{\cdot}OH$ radicals. Also, when the UV-light penetrates the solution, redundant dye molecules prevent the photos from reaching the surface of CuO. It brings on a decrease amount of photons which were adsorbed by CuO and a reduction of degradation efficiency [32, 62–64]. It can be seen that the photodegradation efficiency decreases with the increase of dye concentration when the dosage of CuO remains constant.

In the degradation processes, addition of H_2O_2 is good for the formation of $^{\cdot}OH$, so $^{\cdot}OH$ could probably be the main active species. In order to confirm the conjecture

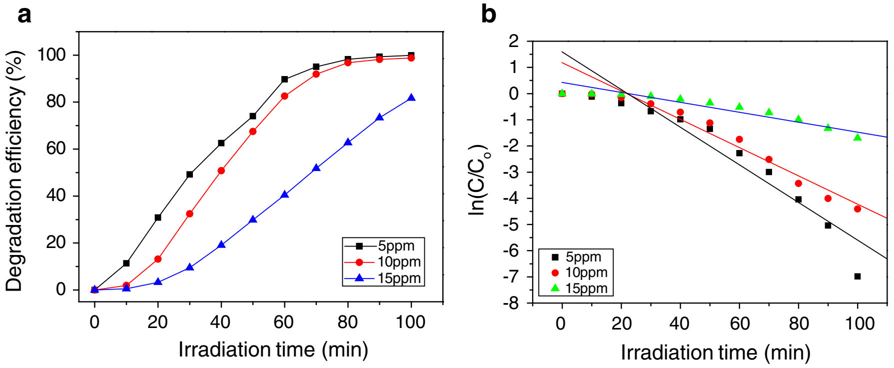

Fig. 12 Degradation of MB versus concentration of MB (**a**) and photodegradation kinetics of MB (**b**); $H_2O_2 = 0.140$ mol L^{-1}; $m_{CuO} = 0.01$ g

above, tert-butyl alcohol (TBA) was used as the hydroxyl radical scavenger [65]. The reaction between the hydroxyl radical and TBA is shown in Eq. (10),

$$(CH_3)_3COH + HO^{\cdot} \rightarrow (CH_3)_3CO^{\cdot} + H_2O_2 \tag{10}$$

Figure 13 illustrates the degradation efficiency with the presence of TBA as radical scavenger at 0.01 g CuO, 0.140 mol L^{-1} H_2O_2 , and 10 mg L^{-1} MB. The degradation efficiency of MB is decreased with the increasing quantity of TBA. Therefore, the results indicate that the hydroxyl radical is an oxidative intermediate and the main active specie in the catalytic degradation of MB. The possible chemical reactions of photodegradation are given as follows [32, 33]:

$$CuO + hv \rightarrow h^{+}_{vB} + e^{-}_{CB} \tag{11}$$

$$H_2O + hv \rightarrow 2HO^{\cdot} \tag{12}$$

$$H_2O_2 + e^{-}_{CB} \rightarrow HO^{\cdot} + OH^{-} \tag{13}$$

$$H_2O + h^{+}_{vB} \rightarrow HO^{\cdot} + H^{+} \tag{14}$$

$$OH^{-} + h^{+}_{vB} \rightarrow HO^{\cdot} \tag{15}$$

$$\text{Dye} + HO^{\cdot} \rightarrow \text{Dye}^{\cdot} \rightarrow \text{degradation products} \tag{16}$$

$$\text{Dye} + h^{+}_{vB} \rightarrow \text{Dye}^{+} \rightarrow \text{degradation products} \tag{17}$$

In order to test the photocatalyst stability of CuO nanoparticles, the catalyst was collected after the degradation process. Then CuO nanoparticles were washed with distilled water and dried at ambient temperature. The collected CuO was reused as the catalyst for the degradation of MB. The data are collected in Table 2. The

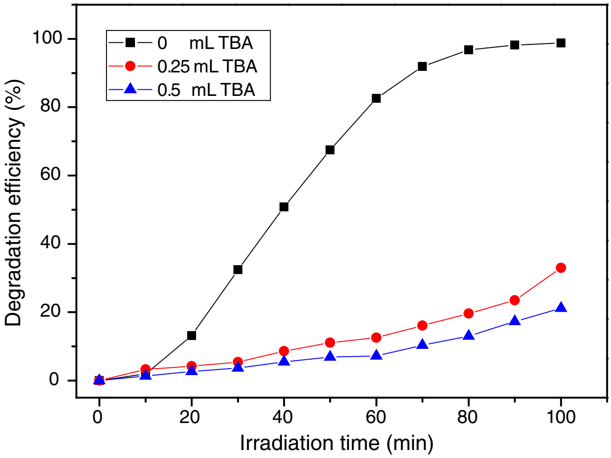

Fig. 13 Effect of radical scavenger (TBA) on the degradation of MB; [MB] = 10 mg L^{-1}; H_2O_{2-} = 0.140 mol L^{-1}; m_{CuO} = 0.01 g

Table 2 Effect of cycle number on the photocatalyst stability of CuO nanoparticles

Cycle number	Degradation efficiency (%)
1	98.63
2	97.67
3	96.42
4	95.27
5	93.98

Reaction conditions: 10 mg CuO samples, 0.140 mol L^{-1} H_2O_2, 70 mL 10 mg L^{-1} MB, 25 °C, 100 min

photocatalyst stability was tested during five runs of photocatalytic reaction and the degradation efficiencies were 98.63, 97.67, 96.42, 95.27, and 93.98 %, respectively. The degradation efficiency is only slightly decreased with the increase of running times. Therefore, CuO nanoparticles are relatively stable photocatalysts.

Conclusion

In this paper, CuO samples have been fabricated by using $CuCO_3 \cdot Cu(OH)_2$ as starting material. In the reaction process, $Cu(OH)_2$ occurred as an intermediate which was converted into CuO at 50 °C for 5 h. The CuO microsphere with about 11.75–12.68 μm in diameter was made up of numerous nanoplates with about 10 nm in thickness. CuO nanoparticles show a good photocatalytic property and photocatalyst stability in the degradation of MB dye under UV-light irradiation.

References

1. L. Vafayi, S. Gharibe, Enhancement of photocatalytic activity of $ZnO–SiO_2$ by nano-sized Pt for efficient removal of dyes from wastewater effluents. Iran. J. Catal. **5**, 365–371 (2015)
2. A. Nezamzadeh-Ejhieh, M. Amiri, CuO supported clinoptilolite towards solar photocatalytic degradation of p-aminophenol. Powder Technol. **235**, 279–288 (2013)
3. A. Nezamzadeh-Ejhieh, M. Karimi-Shamsabadi, Decolorization of a binary azo dyes mixture using CuO incorporated nanozeolite-X as a heterogeneous catalyst and solar irradiation. Chem. Eng. J. **228**, 631–641 (2013)
4. A. Nezamzadeh-Ejhieh, H. Zabihi-Mobarakeh, Heterogeneous photodecolorization of mixture of methylene blue and bromophenol blue using CuO-nano-clinoptilolite. J. Ind. Eng. Chem. **20**, 1421–1431 (2014)
5. A. Fakhri, S. Behrouz, Photocatalytic properties of tungsten trioxide (WO_3) nanoparticles for degradation of lidocaine under visible and sunlight irradiation. Sol. Energy **112**, 163–168 (2015)
6. F. Chen, J.C. Zhao, H. Hidaka, Adsorption factor and photocatalytic degradation of dye-constituent aromatics on the surface of TiO_2 in the presence of phosphate anions. Res. Chem. Intermed. **29**, 733–748 (2003)
7. M.M. Momeni, M. Mirhosseini, M. Chavoshi, A. Hakimizade, The effect of anodizing voltage on morphology and photocatalytic activity of tantalum oxide nanostructure. J. Mater. Sci. Mater. Electron. **27**, 3941–3947 (2016)
8. M.M. Momeni, Y. Ghayeb, Fabrication, characterization and photoelectrochemical performance of chromium-sensitized titania nanotubes as efficient photoanodes for solar water splitting. J. Solid State Electrochem. **20**, 683–689 (2016)

9. E. Sanatgar-Delshade, A. Habibi-Yangjeh, M. Khodadadi-Moghaddam, Hydrothermal low-temperature preparation and characterization of ZnO nanoparticles supported on natural zeolite as a highly efficient photocatalyst. Monatsh. Chem. **142**, 119–129 (2011)
10. M. Sharma, T. Jain, S. Singh, O.P. Pandey, Photocatalytic degradation of organic dyes under UV–Visible light using capped ZnS nanoparticles. Sol. Energy **86**, 626–633 (2012)
11. M. Saranya, R. Ramachandran, E.J.J. Samuel, S.K. Jeong, A.N. Grace, Enhanced visible light photocatalytic reduction of organic pollutant and electrochemical properties of CuS catalyst. Powder Technol. **279**, 209–220 (2015)
12. M.M. Momeni, I. Ahadzadeh, Copper photodeposition on titania nanotube arrays and study of their optical and photocatalytic properties. Mater. Res. Innov. **20**, 44–50 (2016)
13. M.M. Momeni, Y. Ghayeb, Fabrication, characterization and photoelectrochemical behavior of Fe–TiO_2 nanotubes composite photoanodes for solar water splitting. J. Electroanal. Chem. **751**, 43–48 (2015)
14. M.M. Momeni, Y. Ghayeb, Z. Ghonchegi, Fabrication and characterization of copper doped TiO_2 nanotube arrays by in situ electrochemical method as efficient visible-light photocatalyst. Ceram. Int. **41**, 8735–8741 (2015)
15. M.M. Momeni, Y. Ghayeb, Visible light-driven photoelectrochemical water splitting on ZnO–TiO_2 heterogeneous nanotube photoanodes. J. Appl. Electrochem. **45**, 557–566 (2015)
16. M.M. Momeni, Y. Ghayeb, M. Davarzadeh, Single-step electrochemical anodization for synthesis for hierarchical WO_3–TiO_2 nanotube arrays on titanium foil as a good photoanode for water splitting with visible light. J. Electroanal. Chem. **739**, 149–155 (2015)
17. M.M. Momeni, Y. Ghayeb, Photoelectrochemical water splitting on chromium-droped titanium dioxide nanotube photoanodes prepared by single-step anodizing. J. Alloys Compd. **637**, 393–400 (2015)
18. M.M. Momeni, Y. Ghayeb, Preparation of cobalt coated TiO_2 and WO_3–TiO_2 nanotube films via photo-assisted deposition with enhanced photocatalytic activity under visible light illumination. Ceram. Int. **42**, 7014–7022 (2016)
19. M.M. Momeni, Y. Ghayeb, Photochemical deposition of platinum on titanium dioxide-tungsten trioxide nanocomposites: an efficient photocatalyst under visible light irradiation. J. Mater. Sci. Mater. Electron. **27**, 1062–1069 (2016)
20. M.M. Momeni, Y. Ghayeb, Fabrication, characterization and photocatalytic properties of Au/WO_3–TiO_2 nanotubular composite synthesized by photo-assisted deposition and electrochemical anodizing methods. J. Mol. Catal. A Chem. **417**, 107–115 (2016)
21. M.M. Momeni, M. Mirhosseini, M. Chavoshi, Growth and characterization of Ta_2O_5 nanorod and WTa_2O_5 nanowire films on the tantalum substrates by a facile one-step hydrothermal method. Ceram. Int. **42**, 9133–9138 (2016)
22. M.M. Momeni, Y. Ghayeb, Fabrication and characterization of zinc oxide-decorated titania nanoporous by electrochemical anodizing-chemical bath deposition techniques: visible light active photocatalysts with good stability. J. Indian Chem. Soc. **13**, 481–488 (2016)
23. M.M. Momeni, Y. Ghayeb, Cobalt modified tungsten-titania nanotube composite photoanodes for photoelectrochemical solar water splitting. J. Mater. Sci. Mater. Electron. **27**, 3318–3327 (2016)
24. M.M. Momeni, Z. Nazari, Preparation of TiO_2 and WO_3–TiO_2 nanotubes decorated with PbO nanoparticles by chemical bath deposition process: a stable and efficient photo catalyst. Ceram. Int. **42**, 8691–8697 (2016)
25. M.M. Momeni, M. Hakimian, A. Kazempour, In-situ manganese doping of TiO_2 nanostructures via single-step electrochemical anodizing of titanium in an electrolyte containing potassium permanganate: a good visible-light photocatalyst. Ceram. Int. **41**, 13692–13701 (2015)
26. M.M. Momeni, Fabrication of copper decorated tungsten oxide-titanium oxide nanotubes by photochemical deposition technique and their photocatalytic application under visible light. Appl. Surf. Sci. **357**, 160–166 (2015)
27. M.M. Momeni, Highly efficient photoelectrochemical water splitting by a novel nanocomposite titania photoanode. Mater. Res. Innov. **20**, 317–325 (2016)
28. A. Nezamzadeh-Ejhieh, Z. Salimi, Heterogeneous photodegradation catalysis of o-phenylenediamine using CuO/X zeolite. Appl. Catal. A Gen. **390**, 110–118 (2010)
29. A. Nezamzadeh-Ejhieh, Z. Salimi, Solar photocatalytic degradation of o-phenylenediamine by heterogeneous CuO/X zeolite catalyst. Desalination **280**, 281–287 (2011)

30. Q. Zhang, K. Zhang, D. Xu, G. Yang, H. Huang, F. Nie, C. Liu, S. Yang, CuO nanostructures: synthesis, characterization, growth mechanisms, fundamental properties, and applications. Prog. Mater. Sci. **60**, 208–337 (2014)
31. A. Nezamzadeh-Ejhieh, M. Karimi-Shamsabadi, Comparison of photocatalytic efficiency of supported CuO onto micro and nano particles of zeolite X in photodecolorization of methylene blue and methyl orange aqueous mixture. Appl. Catal. A Gen. **477**, 83–92 (2014)
32. K. Mageshwari, R. Sathyamoorthy, J. Park, Photocatalytic activity of hierarchical CuO microspheres synthesized by facile reflux condensation method. Powder Technol. **278**, 150–156 (2015)
33. B. Shaabani, E. Alizadeh-Gheshlaghi, Y. Azizian-Kalandaragh, A. Khodayari, Preparation of CuO nanopowders and their catalytic activity in photodegradation of rhodamine-B. Adv. Powder Technol. **25**, 1043–1052 (2014)
34. Y.X. Zhang, M. Huang, F. Li, Z.Q. Wen, Controlled synthesis of hierarchical CuO nanostructures for electrochemical capacitor electrodes. Int. J. Electrochem. Sci. **8**, 8645–8661 (2013)
35. M. Xu, F. Wang, B. Ding, X. Song, J. Fang, Electrochemical synthesis of leaf-like CuO mesocrystals and their lithium storage properties. RSC Adv. **2**, 2240–2243 (2012)
36. A.V. Nikam, A. Arulkashmir, K. Krishnamoorthy, A.A. Kulkarni, B.L.V. Prasad, pH-Dependent single-step rapid synthesis of CuO and Cu_2O nanoparticles from the same precursor. Cryst. Growth Des. **14**, 4329–4334 (2014)
37. L. Zhu, Y. Chen, Y. Zheng, N. Li, J. Zhao, Y. Sun, Ultrasound assisted template-free synthesis of $Cu(OH)_2$ and hierarchical CuO nanowires from $Cu_7Cl_4(OH)_{10}{\cdot}H_2O$. Mater. Lett. **64**, 976–979 (2010)
38. Y. Zou, Y. Li, X. Lian, D. An, Preparation and characterization of flower-shaped CuO nanostructures by complex precipitation method. Res. Mater. Sci. **3**, 44–51 (2014)
39. Y. Zou, Y. Li, N. Zhang, X. Liu, Flower-like CuO synthesized by CTAB-assisted hydrothermal method. Bull. Mater. Sci. **34**, 967–971 (2011)
40. S. Ghosh, M.K. Naskar, A rapid one-pot synthesis of hierarchical hollow mesoporous CuO microspheres and their catalytic efficiency for the decomposition of H_2O_2. RSC Adv. **3**, 13728–13733 (2013)
41. Z. Cheng, J. Xu, H. Zhong, X. Chu, J. Song, Hydrogen peroxide-assisted hydrothermal synthesis of hierarchical CuO flower-like nanostructures. Mater. Lett. **65**, 2047–2050 (2011)
42. A. Sadollahkhani, Z.H. Ibupoto, S. Elhag, O. Nur, M. Willander, Photocatalytic properties of different morphologies of CuO for the degradation of congo red organic dye. Ceram. Int. **40**, 11311–11317 (2014)
43. Y. Cudennec, A. Lecerf, The transformation of $Cu(OH)_2$ into CuO, revisited. Solid State Sci. **5**, 1471–1474 (2003)
44. M.T.M. Ayob, A.F. Ahmad, H.M.K. Mohd, I.A. Rahman, S. Radiman, Effect of triethanolamine: ethylenediamine ratios on CuO nanoparticles prepared by ultrasound irradiation. AIP Conf. Proc. **1614**, 8–13 (2014)
45. Y. Xu, D. Chen, X. Jiao, Fabrication of CuO pricky microspheres with tunable size by a simple solution route. J. Phys. Chem. B **109**, 13561–13566 (2005)
46. N. Ba, L. Zhu, H. Li, G. Zhang, J. Li, J. Sun, 3D rod-like copper oxide with nanowire hierarchical structure: ultrasound assisted synthesis from $Cu_2(OH)_3NO_3$ precursor, optical properties and formation mechanism. Solid State Sci. **53**, 23–29 (2016)
47. W. Jia, E. Reitz, H. Sun, B. Li, H. Zhang, Y. Lei, From $Cu_2(OH)_3Cl$ to nanostructured sisal-like $Cu(OH)_2$ and CuO: synthesis and characterization. J. Appl. Phys. **105**, 064917 (2009)
48. L.-X. Yang, Y.-J. Zhu, H. Tong, L. Li, L. Zhang, Multistep synthesis of CuO nanorod bundles and interconnected nanosheets using $Cu_2(OH)_3Cl$ plates as precursor. Mater. Chem. Phys. **112**, 442–447 (2008)
49. A.A. Novikova, D.Y. Moiseeva, E.V. Karyukov, A.A. Kalinichenko, Facile preparation photocatalytically active CuO plate-like nanoparticles from brochantite. Mater. Lett. **167**, 165–169 (2016)
50. W. Jia, E. Reitz, H. Sun, H. Zhang, Y. Lei, Synthesis and characterization of novel nanostructured fishbone-like $Cu(OH)_2$ and CuO from $Cu_4SO_4(OH)_6$. Mater. Lett. **63**, 519–522 (2009)
51. L. Zhang, J.C. Yu, A.-W. Xu, Q. Li, K.W. Kwong, S.-H. Yu, Peanut-shaped nanoribbon bundle superstructures of malachite and copper oxide. J. Cryst. Growth **266**, 545–551 (2004)
52. C. Zhu, C. Chen, L. Hao, Y. Hu, Z. Chen, In-situ preparation of 1D CuO nanostructures using $Cu_2(OH)_2CO_3$ nanoribbons as precursor for sacrifice-template via heat-treatment. Solid State Commun. **130**, 681–686 (2004)
53. T.X. Wang, S.H. Xu, F.X. Yang, Green synthesis of CuO nanoflakes from $CuCO_3{\cdot}Cu(OH)_2$ powder and H_2O_2 aqueous solution. Powder Technol. **228**, 128–130 (2012)

54. C. Lu, L. Qi, J. Yang, D. Zhang, N. Wu, J. Ma, Simple template-free solution route for the controlled synthesis of $Cu(OH)_2$ and CuO nanostructures. J. Phys. Chem. B **108**, 17825–17831 (2004)
55. H. Wang, J.-Z. Xu, J.-J. Zhu, H.-Y. Chen, Preparation of CuO nanoparticles by microwave irradiation. J. Cryst. Growth **244**, 88–94 (2002)
56. M. Karimi-Shamsabadi, A. Nezamzadeh-Ejhieh, Comparative study on the increased photoactivity of coupled and supported manganese-silver oxides onto a natural zeolite nano-particles. J. Mol. Catal. A Chem. **418**, 103–114 (2016)
57. W. Wang, L. Wang, H. Shi, Y. Liang, A room temperature chemical route for large scale synthesis of sub-15 nm ultralong CuO nanowires with strong size effect and enhanced photocatalytic activity. Cryst. Eng. Comm. **14**, 5914–5922 (2012)
58. S. Azimi, A. Nezamzadeh-Ejhieh, Enhanced activity of clinoptilolite-supported hybridized PbS–CdS semiconductors for the photocatalytic degradation of a mixture of tetracycline and cephalexin aqueous solution. J. Mol. Catal. A Chem. **408**, 152–160 (2015)
59. A. Nezamzadeh-Ejhieh, Z. Banan, Kinetic investigation of photocatalytic degradation of dimethyldisulfide by zeolite a containing nano CdS. Iran. J. Catal. **2**, 79–83 (2012)
60. M. Amiri, A. Nezamzadeh-Ejhieh, Improvement of the photocatalytic activity of cupric oxide by deposition onto a natural clinoptilolite substrate. Mater. Sci. Semicond. Process. **31**, 501–508 (2015)
61. C. Han, H. Yang, X. Xue, Kinetics of photocatalytic degradation of methylene blue over $CaTiO_3$. J. Wuhan Univ. Technol. Mater. Sci. Ed. **30**, 1103–1107 (2015)
62. A.N. Ejhieh, M. Khorsandi, Photodecolorization of eriochrome black T using Nis-P zeolite as a heterogeneous catalyst. J. Hazard. Mater. **176**, 629–637 (2010)
63. A. Nezamzadeh-Ejhieh, S. Hushmandrad, Solar photodecolorization of methylene blue by CuO/X zeolite as a heterogeneous catalyst. Appl. Catal. A Gen. **388**, 149–159 (2010)
64. A. Nezamzadeh-Ejhieh, N. Moazzeni, Sunlight photodecolorization of a mixture of methyl orange and bromocresol green by CuS incorporated in a clinoptilolite zeolite as a heterogeneous catalyst. J. Ind. Eng. Chem. **19**, 1433–1442 (2013)
65. F. Ahmedchekkat, M.S. Medjram, M. Chiha, A.M.A. Albsoul, Sonophotocatalytic degradation of rhodamine B using a novel reactor geometry: effect of operating conditions. Chem. Eng. J. **178**, 244–251 (2011)